ChemPubSoc Europe

DOI: 10.1002/cplu.201402050

Enhanced Wave-Absorption Properties of Nanocomposites Based on the Synthesized Bi_2S_3 Nanorods and Polyvinylidene Fluoride

Xin Luo,[a] Guang-Sheng Wang,*[a] Hao-Yue Guo,[a] Xiao-Juan Zhang,[a] Wen-Qiang Cao,[b] Yun-Zhao Wei,[a] Lin Guo,[a] and Mao-Sheng Cao*[b]

In this study, Bi_2S_3 nanorods were synthesized on a large scale through a simple hydrothermal method at low temperature. To investigate the wave-absorption properties of Bi_2S_3 nanorods, the homogeneous nanocomposites consisting of the nanorods and paraffin or polyvinylidene fluoride (PVDF) matrix were fabricated and characterized. The results indicated that the introduction of Bi_2S_3 nanorods to PVDF significantly enhanced the wave-absorption properties of the absorber. The loss mechanism of Bi_2S_3/PVDF nanocomposites with different loadings was discussed and some theories were also employed to explain the mechanism of the enhancement based on the experimental results.

Introduction

Electromagnetic radiation pollution has been recognized worldwide as the fourth major pollutant after water, atmospheric, and noise pollution. Owing to the invisible nature of electromagnetic radiation pollution, its damage is often underestimated. To prevent electromagnetic interference and damage to health as well as to provide electromagnetic protection for civilian facilities, it is necessary to develop new types of wave-absorbing and antistatic materials. In addition, with the development of detection technology and precision-guided munitions in military affairs, better stealth technologies are needed to protect armaments. At present, traditional absorbing materials cannot meet the requirements of the military. Excellent wave-absorbing materials are supposed to be broadband, lightweight, and simple-structured with strong absorption. Nevertheless, traditional wave-absorbing materials generally reduce electromagnetic waves through dielectric and magnetic loss processes, and are usually only able to perform strong absorption in some narrow frequency band. Furthermore, inorganic absorbers have a high density and are scarcely able to meet the requirement of lightweight.

Over the past fifteen years, the preparation and assembly techniques of nanomaterials have been well developed. But as an emerging functional material, the research into its application is still insufficient and is regarded as a hot topic for scientists. Their special structures make nanomaterials distinct from most common inorganic fillers in their physical properties, and researchers can make the most of this to expand their range of applications.

In recent years, wave-absorbing nanomaterials have attracted increasing attention as a new kind of functional material with excellent performance.[1,2] Nevertheless, nanostructured wave-absorbing materials alone do not satisfy the requirements for their practical application. Currently, the top challenge in this field is how to achieve broadband absorption, which requires not only approximate electromagnetic parameters, but also adequate parameter stabilities and disperse characteristics.[3–5] However, to attain light, thin, and compatible wave-absorbing materials, advanced material and technology must be applied. Thus, it has become an important task to develop high-performance material systems with controllable electromagnetic parameters in the field of stealth materials.

At present, many research teams have discovered the special electromagnetic characteristics of nanomaterials and some of them have reported remarkable achievements.[6] Watts et al. reported the conductivity and permeability behavior of carbon-nanotube nanocomposites that have notable high permittivity and permeability in the X band (8–12 GHz).[7,8] Terada et al. studied the wave-absorption property of Fe_3C/carbon nanocomposites and obtained materials with absolute reflection loss over 20 dB in the frequency 6–14 GHz for the absorbers with a respective thickness of 1.5–3 mm.[9] Liu et al. developed ferric nanowire nanocomposites possessing an absolute reflection loss over 20 dB at 5.6–18 GHz with an absorber thickness of 1.3–4.0 mm and up to 47 dB at 9.4 GHz with a thickness of 2 mm.[10] Chen et al. discovered that a zinc oxide nanowire/polyester nanocomposite possesses a relatively good electromagnetic wave-absorption property in the X band.[11] A study by Zhou et al. showed that a zinc oxide nanowhisker nanocomposite coating displays a favorable wave-absorption property, which could be adjusted by changing the loading or morphology of the nanowhisker.[12] Wu and Kong investigated the dielectric property of a multiwalled carbon nanotube (MWCNT) nanocomposite under high frequency. The results showed that as the loading of the MWCNTs rises, the dielectric constants of

[a] X. Luo, Dr. G.-S. Wang, H.-Y. Guo, X.-J. Zhang, Y.-Z. Wei, Prof. L. Guo
Key Laboratory of Bio-Inspired Smart Interfacial Science and Technology of Ministry of Education
School of Chemistry and Environment
Beihang University, Beijing 100191 (P.R. China)
E-mail: wanggsh@buaa.edu.cn

[b] W.-Q. Cao, Prof. M.-S. Cao
School of Materials Science and Engineering
Beijing Institute of Technology
Beijing 100081 (P.R. China)
E-mail: caomaosheng@bit.edu.cn

Supporting information for this article is available on the WWW under http://dx.doi.org/10.1002/cplu.201402050.

the nanocomposite increases and the dielectric relaxation and conductivity are reinforced, which shows a high dielectric response.[13] In recent years, lower-dimensional materials such as Fe_3O_4,[14,15] ZnO,[16] CdS/Fe_2O_3,[17] MnO_2,[18] and so forth stepped onto the stage of wave-absorbing materials and revealed extraordinary properties. Our research team recently discovered that the complex symmetrical CuS nanostructure has superior wave-absorption property[19,20] as well as the phenomenon that a conductor and semiconductor can generate a synergistic effect and enhance the wave-absorption property.[21,22]

In this study, we synthesized a one-dimensional bismuth sulfide nanomaterial on a large scale through a simple hydrothermal method.[23] Then, Bi_2S_3/paraffin and Bi_2S_3/polyvinylidene fluoride (PVDF) were fabricated to investigate the electromagnetic parameters and absorption properties of the nanocomposites. We made a special effort to investigate and study the relationship between the change of filler loadings and properties and to try to reveal the variation rules of the wave-absorption property as well as the enhancement mechanism.

Results and Discussion

The phase purity and crystal structure of the Bi_2S_3 nanorods were examined by XRD, as shown in Figure 1. All of the peaks match well with Bragg diffractions, and all of the diffraction

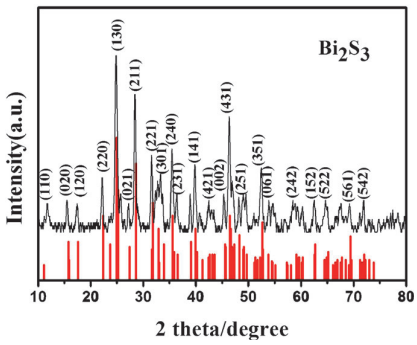

Figure 1. XRD pattern of the as-synthesized Bi_2S_3 nanorods.

peaks can be exclusively indexed to a pure orthorhombic phase of Bi_2S_3 with lattice parameters of $a = 11.13$ Å, $b = 11.28$ Å, and $c = 3.979$ Å (space group: $Fm3m$), which matches well with the reported values (JCPDS 17-0320) shown in red. No peaks for other phases were detected, which indicates the high purity and crystallinity of the samples obtained as reported.

The morphologies of the as-synthesized Bi_2S_3 are revealed by the SEM image in Figure 2a. It is observed that the products are Bi_2S_3 nanorods with a typical length of about 1 to 2 μm with some other shorter rods of different lengths, which seem to be fragments of the longer ones.[24] The diameter of the rods ranges from 90 to 120 nm. Figure 2b shows the field-emission scanning electron microscopy (FESEM) image of the product and the elemental maps of Bi and S in the rectangular area. The density of points in a different color for each element

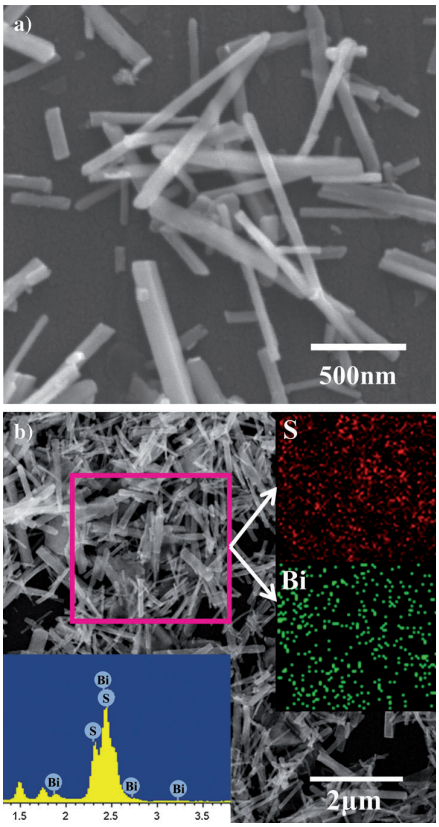

Figure 2. a) SEM image of the as-synthesized Bi_2S_3 nanorods. b) FESEM image of the Bi_2S_3 nanorods with the corresponding elemental mapping images of S and Bi and the EDX elemental analysis.

suggests the stoichiometric ratio of the two elements in this compound, which can also be calculated from the energy-dispersive X-ray analysis (EDAX) spectrum at the bottom left of Figure 2b.

As demonstrated in Figure S1 in the Supporting Information, the nanocomposite membrane of Bi_2S_3/PVDF obtained through the method reported herein inherits the processability and flexibility of the polymer. In this study, several characterization approaches were employed to reveal the structure and morphology of the membranes along with a good dispersion of Bi_2S_3 particles in the polymer matrix.

Figure 3a presents the XRD patterns of the as-prepared nanocomposite membranes loaded with Bi_2S_3 nanorods of 10, 20, 30, and 40 wt% content. As shown in Figure 3, some diffraction maxima of the Bi_2S_3 powder vanished or decreased after being mixed into PVDF, such as the crystal faces (211), (351), and (431). At the same time, some of the other main maxima such as (130), (240), and (220) were still present and some were even enhanced. These transformations may be ascribed to the embedding effect of the polymer matrix and are also very possibly related to the tendency of the directional alignment of the nanorods.[22]

To study the inner structure of the nanocomposites, the membrane with a filler content of 40 wt% was fractured in an environment of low temperature provided by liquid nitrogen.

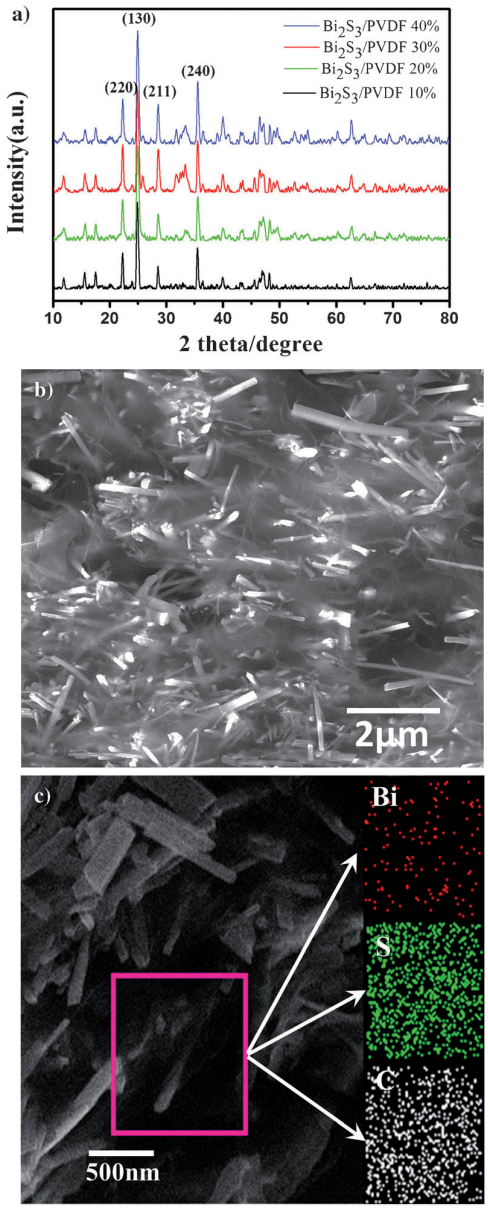

Figure 3. a) XRD patterns of the Bi_2S_3/PVDF nanocomposite membranes loaded with Bi_2S_3 nanorods of 10, 20, 30, and 40 wt%. b) SEM micrograph of the fracture surface of the nanocomposite membrane. c) EDAX elemental maps of Bi, S, and C on the fracture surface.

Afterwards, SEM and EDX analyses was carried out on the fracture surface. Figure 3b shows the micrograph of the fractured surface; it shows that Bi_2S_3 nanorods interlace with each other and most are parallel to the surface of the film. The fuzzy parts throughout are attributable to the PVDF matrix. The EDAX elemental maps of Bi and S, in the nanoparticles, and C, in the polymer, are presented in Figure 3c, which illustrates the homogeneous dispersion of the Bi_2S_3 nanorods in the PVDF matrix. This result was also confirmed by the EDAX element spectrum of the fractured surface, which is shown in Figure S2 in the Supporting Information.

In this study, the wave-absorption properties of the materials were generally measured by the reflection loss (RL) coefficients as was done in many of our former studies and other reports.[18–22,25] The RL coefficients of pure PVDF and the nanocomposites were calculated by using the measured relative complex permittivity and permeability values. According to the transmission line theory, the RL coefficient (dB) of an electromagnetic wave under the normal incidence at the surface of a single-layer material backed by a perfect conductor at a given frequency and material thickness can be calculated through Equations (1) and (2):[26]

$$Z_{in} = \sqrt{\frac{\mu_r}{\varepsilon_r}} \tanh\left[j\left(\frac{2f\pi d}{c}\right)\sqrt{\mu_r \varepsilon_r}\right] \quad (1)$$

$$R = 20\log\left|\frac{Z_{in}-1}{Z_{in}+1}\right| \quad (2)$$

in which Z_{in} is the input impedance of the absorber, R represents the reflection loss, ε_r is the complex permittivity, μ_r is the relative complex permeability (the μ_r values of Bi_2S_3 are regarded as 1, given that the material possesses no notable magnetism), f is the frequency of the microwaves, d is the thickness of the absorber, and c is the velocity of light in a vacuum.

Figure 4 shows the calculated theoretical RLs of the Bi_2S_3/paraffin nanocomposites with different loadings (10, 20, and 40 wt%) and different thicknesses in the frequency range of 2–18 GHz. Since a paraffin matrix is transparent to microwaves, these results are generally regarded as the wave-absorption capacities of the filler itself (that is, Bi_2S_3 in this study) for further comparison with other nanocomposites. As is illustrated in Figure 4a–c, the RLs of the Bi_2S_3/paraffin nanocomposites vary distinctly at different microwave frequencies and absorber thicknesses, and generate absorption peaks in the figure. Nevertheless, the values of the RLs are rather high; the minimum is only about −4 dB of 10 and 20 wt% loaded nanocomposites and about −7 dB of 40 wt% loaded ones. Moreover, the RLs increase slowly with the increase of the Bi_2S_3 content in paraffin according to the results, which can be more concisely observed in Figure 4d for the RL curves of Bi_2S_3/paraffin nanocomposites with different loadings and the same thickness of 3.5 mm.

In the same way, RL values in the frequency range of 2–18 GHz for Bi_2S_3/PVDF nanocomposites with different thicknesses and loadings were obtained and are demonstrated in Figure 5a–c. The calculations of Bi_2S_3/PVDF and Bi_2S_3/paraffin nanocomposites with different loadings and the same thickness of 3.5 mm are also showed in Figure 5d for comparison. On the one hand, the wave-absorption properties are remarkably enhanced after replacing paraffin with PVDF in the nanocomposites, which can be observed directly in Figure 5d. The maximum RL reaches −32 (10 wt% at 10.7 GHz), −22 (20 wt% at 9.0 GHz), and −29 dB (40 wt% at 13.4 GHz) and instead of large areas, intensive absorptions arise in some narrow range of frequency and thickness, which result in sharp peaks in the diagrams. On the other hand, as more Bi_2S_3 nanorods are

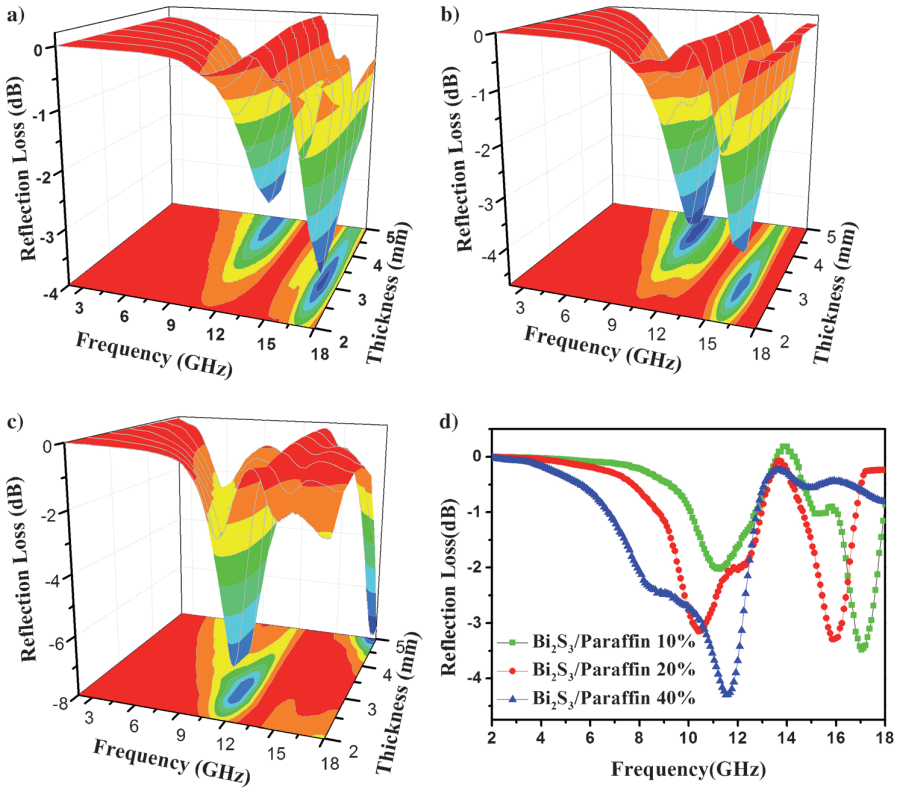

Figure 4. Reflection losses of Bi_2S_3/paraffin at various thicknesses in the frequency range of 2–18 GHz with different loadings of a) 10, b) 20, and c) 40 wt%. d) RL curves of Bi_2S_3/paraffin nanocomposites with different loadings and same thickness of 3.5 mm.

added to PVDF, the Bi_2S_3/PVDF nanocomposites tend to show absorptions in broader areas or as series of sharp peaks like the diagram in Figure 5c. According to Figure 5e, Bi_2S_3/PVDF nanocomposites with 40 wt% loading attained a reflection loss of less than −10 dB in the frequency range from 3.6 to 17.0 GHz with an absorber thickness of 2.0–5.0 mm, which is generally considered to be a broadband wave-absorbing material.[9,10] The enlargement of the absorption range is quite beneficial to many electromagnetic shielding materials that are supposed to reduce electromagnetic waves over a wide frequency range. In addition, the frequency of the minimum RLs, corresponding to the maximum absorptions, can be tuned by altering the absorber thickness. As the absorber thickness increases, the minimum RL frequency tends to shift toward lower values.

The relationship between the Bi_2S_3 nanorod loadings in PVDF and the RLs of the samples remains vague on the basis of the acquired results so far. Different from Bi_2S_3/paraffin, the RLs did not increase when more nanorods were added to the nanocomposites; the enhancement in wave-absorption property of Bi_2S_3/PVDF was more apparent when the loading was relatively lower, which means that samples with lower loadings possess higher maximum absorptions (−32 dB for 10 wt%). As a larger amount of Bi_2S_3 is introduced into the system, the maximum absorption decreases at the beginning (−22 dB for 20 wt%) and then it rises slowly (−29 dB for 40 wt%), which is different from most of our former studies.[19,20] The variation can also be observed in the RL curves of Bi_2S_3/PVDF nanocomposites with different loadings and the same thickness of 3.5 mm as shown in Figure 5d. From another perspective, samples with higher loadings tend to consume waves in broader frequency ranges. These results indicate that the microwave loss mechanism of Bi_2S_3/PVDF nanocomposites is substantially complex and far more than the numerical addition of Bi_2S_3/paraffin and pure PVDF.

The dielectric loss, generally concerning the dipolar polarization and electric polarization of the mesoscopic and microscopic structures of a material, plays a significant role in the wave-absorption properties of dielectric media.[27] Figure 6 presents the frequency-dependent real (ε') and imaginary (ε'') parts of the complex permittivity of the two nanocomposites with various Bi_2S_3 loadings. The real part of the permittivity indicates the polarization extents, and the dielectric loss is calculated through dividing the imaginary part by the real part. The dielectric loss tangents of both Bi_2S_3/paraffin and Bi_2S_3/PVDF with different loadings are demonstrated in Figure S3 in the Supporting Information. In Figure 6a, the nanocomposites with a higher mass percentage of Bi_2S_3 nanorods clearly attain a higher real permittivity, both in Bi_2S_3/paraffin and Bi_2S_3/PVDF. A similar connection can be recognized in the imaginary permittivity curve in Figure 6b, except that high imaginary permittivities at different frequencies emerge as the loading changes. Furthermore, both the real and imaginary parts of the permittivity are significantly enhanced when fabricating the nanocomposite of Bi_2S_3/PVDF compared with pure PVDF. This phenomenon is generally ascribed to a synergistic effect, which proposes that the mutual effect between the components of the nanocomposite creates additional microwave loss mechanisms.

Debye dipolar relaxation is a crucial mechanism through which the inorganic–organic composite can absorb microwaves, as reported in our former studies.[18,19,21] In a Debye relaxation process, the relationship between the real part (ε') and imaginary part (ε'') could be expressed by Equation (3).[19,25,28]

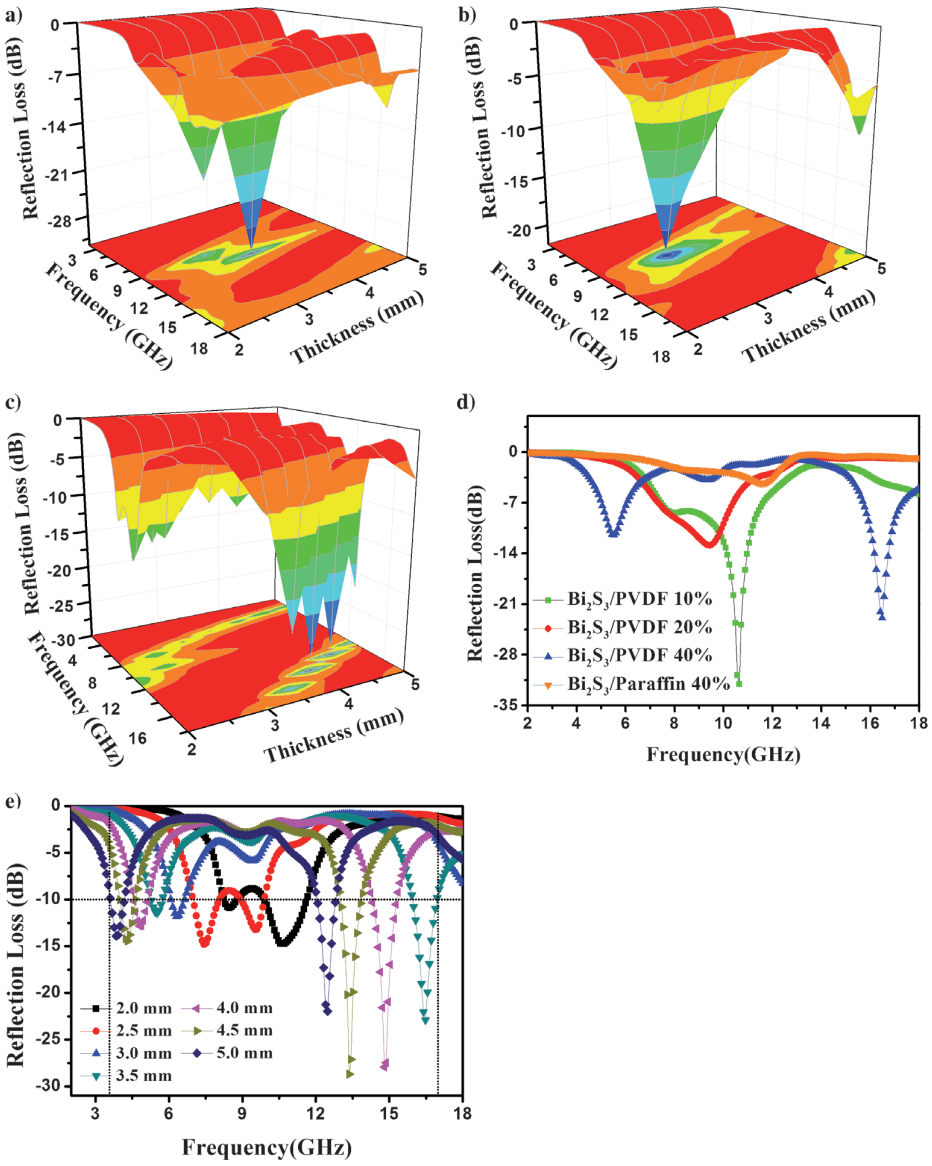

Figure 5. Reflection losses of Bi_2S_3/PVDF at various thicknesses in the frequency range of 2–18 GHz with different loadings of a) 10, b) 20, and c) 40 wt%. d) Reflection loss curves of Bi_2S_3/PVDF and Bi_2S_3/paraffin nanocomposites with different loadings and the same thickness of 3.5 mm. e) Reflection loss curves of 40 wt%-loaded Bi_2S_3/PVDF at various thicknesses in the frequency range of 2–18 GHz.

$$\left(\varepsilon' - \frac{\varepsilon_s + \varepsilon_\infty}{2}\right)^2 + (\varepsilon'')^2 = \left(\frac{\varepsilon_s + \varepsilon_\infty}{2}\right)^2 \quad (3)$$

in which ε_s and ε_∞ are the static permittivity and relative dielectric permittivity at the high-frequency limit, respectively. Thus, the plot of ε' versus ε'' would be a single semicircle, generally denoted as the Cole–Cole semicircle. The ε'–ε'' curves of pure PVDF are demonstrated in Figure S4 and the ε'–ε'' curves of different nanocomposite samples are given in Figure S5. As presented in Figure S5, several semicircles can be recognized in each diagram, which indicates the universal existence and vital function of Debye relaxation in wave-absorption processes. There is also one semicircle observed in Figure S4, which suggests that this relaxation process may also exist in pure PVDF. The increase of nanocomposite loadings apparently changes the relaxation process, but the connection remains unclear.

Maxwell–Wagner relaxation is another loss mechanism in wave-absorption processes.[25,28] In heterogeneous media like nanocomposites, charges accumulate at the interfaces and large dipoles form on particles or clusters. When electromagnetic waves propagate in the nanocomposites, the interfacial polarization (also called the Maxwell–Wagner effect) consumes a lot of waves. The interfaces between the Bi_2S_3 nanorods and PVDF formed in the nanocomposites during the synthesis process. Thus, Maxwell–Wagner relaxation is one of the factors that lead to a better wave-absorption property (both maximum absorption and the range) with higher loadings.

In addition, free-electron theory reveals that [Eq. (4)]:

$$\varepsilon'' \propto \frac{\sigma}{2\pi\varepsilon_0 f} \quad (4)$$

in which σ is the electrical conductivity. The relationship indicates that an increased conductivity of composites results in a stronger dielectric loss. Semiconductor Bi_2S_3 has relatively good electrical conductivity, thus the addition of Bi_2S_3 shall result in considerable enhancement in the conductivity of the fabricated Bi_2S_3/PVDF nanocomposite and lead to better wave-absorption properties.

Conclusion

Wave-absorption properties were studied by comparison of the nanocomposites of Bi_2S_3/paraffin and Bi_2S_3/PVDF with the same filler loadings. The results confirmed that the introduction of Bi_2S_3 nanorods to PVDF can significantly enhance the wave-absorption property of the nanocomposites. Samples with relatively lower loadings were found to exhibit a better maximum absorption (−32 dB for 10 wt% at 10.7 GHz); as

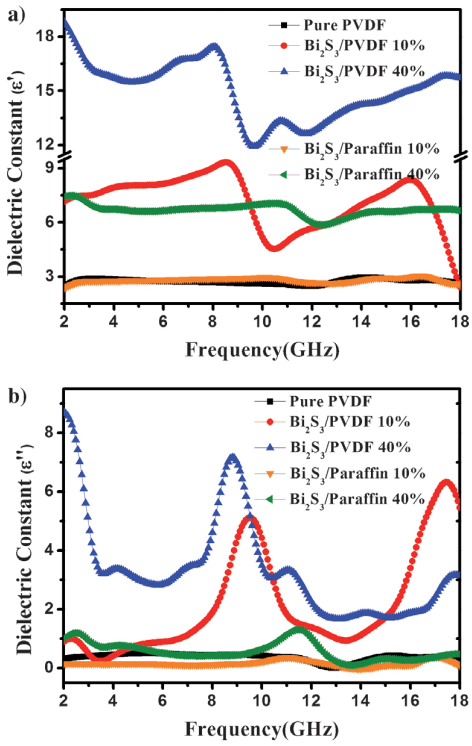

Figure 6. Measured frequency-dependent a) real parts and b) imaginary parts of the complex permittivity of different samples.

a larger amount of Bi_2S_3 was added to the system, the maximum absorption decreased at the beginning (−22 dB for 20 wt% at 9.0 GHz) and then increased slowly (−29 dB for 40 wt% at 13.4 GHz). The reflection loss of the Bi_2S_3/PVDF nanocomposite with 40 wt% loading reached less than −10 dB in the frequency range from 3.6 to 17.0 GHz with an absorber thickness of 2.0–5.0 mm, which shows it to be a promising broadband wave-absorbing material. Finally, loss mechanisms of Bi_2S_3/PVDF with different loadings were discussed depending on their dielectric behaviors. The enhancement mechanism of the wave-absorption properties is generally ascribed to Debye dipolar relaxation, Maxwell–Wagner relaxation, and electron polarization in the system.

Experimental Section

All of the reactants and solvents were of analytical grade and were used without further purification.

Synthesis of Bi_2S_3 nanorods

The bismuth sulfide nanorods were synthesized by the reaction of bismuth chloride ($BiCl_3$) and sodium sulfide (Na_2S) in a homogeneous aqueous solution, as was reported in a former study.[23] To be precise, $BiCl_3$ (1.9 g, 6 mmol) was added to deionized water (8 mL) with agitation, and concentrated hydrochloric acid (HCl, 36%, ca. 2 mL) was added dropwise to dissolve the white precipitate (BiOCl) generated in the previous step. Separately, sodium sulfide ($Na_2S{\cdot}9H_2O$; 2.4 g, 10 mmol) was dissolved in deionized water (5 mL). Finally, these two solutions were mixed in a 100 mL Teflon-lined stainless-steel autoclave, sealed and maintained at 180 °C for 12 h. After that, the mixture was cooled to room temperature naturally and the solid product was filtered, and washed with deionized water and absolute ethanol several times. Finally the obtained sample was dried in air.

Preparation of Bi_2S_3/paraffin and Bi_2S_3/PVDF nanocomposites

To measure the microwave-absorption properties of the pure Bi_2S_3 nanorods, the specimens were prepared by adding the product to a paraffin matrix, which is transparent to microwaves, through heating and an ultrasonic dispersion method. The Bi_2S_3/PVDF nanocomposite was prepared by dispersing and dissolving the desired amount of sample powder as well as the PVDF powder together in *N*,*N*-dimethylformamide (DMF; 30 mL) under magnetic stirring. After repetitious agitation and ultrasonic dispersion for about 2 h, the mixture was poured onto a glass culture dish and dried at 80 °C for 24 h to form a thin film.

Characterization

The purity and crystalline structure of the products were confirmed by XRD analyses, recorded on a (Philips X'Pert Pro Super) X-ray powder diffractometer with $Cu_{K\alpha}$ radiation ($\lambda = 0.154056$ nm). The grain morphology and size were observed by sputtering with gold for SEM on a KYKY-1010B microscope and FESEM on a JSM-6700F microscope. In addition, EDX measurements were conducted on an electron spectroscopy for chemical analysis ESCAPlus spectrometer from Oxford Instruments.

Those two nanocomposites were pressed to form hollow cylindrical compacts ($\Phi_{out} = 7.00$ mm, $\Phi_{in} = 3.04$ mm) in a mold under 4–6 MPa for the microwave-absorption measurement. The processing of Bi_2S_3/PVDF film should be in a heated environment at 220 to 230 °C. Maintain the temperature and pressure conditions for around 5 min, and then cool it in the natural way to room temperature. Then the relative permittivity values were measured in the range of 2–18 GHz through a coaxial wire method using an Anritsu 37269D network analyzer.

Acknowledgements

This project was financially supported by the National Basic Research Program of China (2010CB934700) and the National Natural Science Foundation of China (nos. 51102223, 50725208, and 51132002).

Keywords: absorption · bismuth · hydrothermal synthesis · nanostructures · polymers

[1] R. Kumar Srivastava, T. N. Narayanan, A. P. Reena Mary, M. R. Anantharaman, A. Srivastava, R. Vajtai, P. M. Ajayan, *Appl. Phys. Lett.* **2011**, *99*, 113116.
[2] C. Wang, X. Han, P. Xu, X. Zhang, Y. Du, S. Hu, J. Wang, X. Wang, *Appl. Phys. Lett.* **2011**, *98*, 072906.
[3] M. Cao, R. Qin, C. Qiu, J. Zhu, *Mater. Des.* **2003**, *24*, 391–396.
[4] M. Cao, B. Wang, Q. Li, J. Yuan, G. Xu, S. Qin, X. Fang, *Mater. Des.* **1998**, *19*, 113–120.
[5] M. Cao, J. Zhu, J. Yuan, T. Zhang, Z. Peng, Z. Gao, G. Xiao, S. Qin, *Mater. Des.* **2002**, *23*, 557–564.

[6] J. Zhou, S. Zhou, Q. Zhang, G. Shen, D. Xia, J. Huang, *Synth. React. Inorg., Met.-Org., Nano-Met. Chem.* **2012**, *42*, 392 – 397.
[7] P. C. P. Watts, D. R. Ponnampalam, W. K. Hsu, A. Barnes, B. Chambers, *Chem. Phys. Lett.* **2003**, *378*, 609 – 614.
[8] P. C. P. Watts, W. K. Hsu, A. Barnes, B. Chambers, *Adv. Mater.* **2003**, *15*, 600 – 603.
[9] M. Terada, M. Itoh, J. R. Liu, K.-i. Machida, *J. Magn. Magn. Mater.* **2009**, *321*, 1209 – 1213.
[10] J. R. Liu, M. Itoh, M. Terada, T. Horikawa, K.-i. Machida, *Appl. Phys. Lett.* **2007**, *91*, 093101.
[11] Y. J. Chen, M. S. Cao, T. H. Wang, Q. Wan, *Appl. Phys. Lett.* **2004**, *84*, 3367.
[12] Z. Zhou, S. Liu, L. Gu, *J. Appl. Polym. Sci.* **2001**, *80*, 1520 – 1525.
[13] J. Wu, L. Kong, *Appl. Phys. Lett.* **2004**, *84*, 4956.
[14] J. Liu, R. Che, H. Chen, F. Zhang, F. Xia, Q. Wu, M. Wang, *Small* **2012**, *8*, 1214 – 1221.
[15] G. Wang, Z. Gao, S. Tang, C. Chen, F. Duan, S. Zhao, S. Lin, Y. Feng, L. Zhou, Y. Qin, *ACS Nano* **2012**, *6*, 11009 – 11017.
[16] X. G. Liu, J. J. Jiang, D. Y. Geng, B. Q. Li, Z. Han, W. Liu, Z. D. Zhang, *Appl. Phys. Lett.* **2009**, *94*, 053119.
[17] X. L. Shi, M. S. Cao, J. Yuan, Q. L. Zhao, Y. Q. Kang, X. Y. Fang, Y. J. Chen, *Appl. Phys. Lett.* **2008**, *93*, 183118.
[18] G. S. Wang, S. He, X. Luo, B. Wen, M. M. Lu, L. Guo, M. S. Cao, *RSC Adv.* **2013**, *3*, 18009 – 18015.
[19] S. He, G. S. Wang, C. Lu, J. Liu, B. Wen, H. Liu, L. Guo, M. S. Cao, *J. Mater. Chem. A* **2013**, *1*, 4685 – 4692.
[20] S. He, G. S. Wang, C. Lu, X. Luo, B. Wen, L. Guo, M. S. Cao, *ChemPlusChem* **2013**, *78*, 250 – 258.
[21] X. J. Zhang, G. S. Wang, Y. Z. Wei, L. Guo, M. S. Cao, *J. Mater. Chem. A* **2013**, *1*, 12115 – 12122.
[22] G. S. Wang, Y. Z. Wei, C. Lu, Y. H. Yue, J. Wu, L. Guo, *J. Mater. Chem. A* **2014**, *2*, 5516 – 5524.
[23] J. Lu, Q. Han, X. Yang, L. Lu, X. Wang, *Mater. Lett.* **2007**, *61*, 3425 – 3428.
[24] Y. Deng, Y. Zhang, Y. Xiang, G. Wang, H. Xu, *J. Mater. Chem.* **2009**, *19*, 2058 – 2061.
[25] D. Chen, G. S. Wang, S. He, J. Liu, L. Guo, M. S. Cao, *J. Mater. Chem. A* **2013**, *1*, 5996 – 6003.
[26] M. S. Cao, X. L. Shi, X. Y. Fang, H. B. Jin, Z. L. Hou, W. Zhou, Y. J. Chen, *Appl. Phys. Lett.* **2007**, *91*, 203110.
[27] X. F. Zhang, X. L. Dong, H. Huang, Y. Y. Liu, W. N. Wang, X. G. Zhu, B. Lv, J. P. Lei, C. G. Lee, *Appl. Phys. Lett.* **2006**, *89*, 053115.
[28] P. K. Mandal, A. Lapanik, R. Wipf, B. Stuehn, W. Haase, *Appl. Phys. Lett.* **2012**, *100*, 073112.

Received: March 5, 2014
Published online on May 14, 2014